Adiabatic heating and role of the intermetallic phase on the ECAP-induced strengthening in an Al-Cu alloy

M. Cabibbo

In the present work, the strengthening effect of the Fe-rich intermetallic phases in a 2219 aluminum alloy subjected to equal-channel angular pressing (ECAP) has been studied. Three different deformation conditions, corresponding to the as-extruded, ECAP/A-1 pass and ECAP/A-2 passes were considered. Mechanical and morphological characterizations have been performed by microhardness tests, light microscopy, transmission electron microscopy and scanning electron microscopy observations. All the contributions to the strengthening due to solid solution, dislocation boundary and secondary phase have been discussed. The electron microscopy study focused on the evaluation of the strengthening effect generated by the $(Fe,Mn,Cr)_3Si_2Al_{15}$ intermetallic. This strengthening effect, generated by coarse precipitates such are the Fe-rich intermetallics, has also been correlated to the morphological particle aspect. The ECAP-induced adiabatic heating strengthening contribution was also determined. A strengthening combination model of all the microstructure terms was proposed and applied to this case to meet the alloy yield stress at the two different ECAP straining levels corresponding to the first and the second pass via route A.

Keywords: Intermetallic phase - ECAP - Strengthening - Al-Cu alloy

INTRODUCTION

The subdivision of crystals and grains during deformation takes place as deformation bands, on a macroscopic scale, and as cell blocks and cells, on a smaller scale. At increasing stress and strain this microstructure boundary subdivision takes place on a finer and finer scale, with the rate strongly dependingupon the deformation process used. The refinement of the microstructure is accompanied by an increase in the average angle across both grain and cell boundaries [1]. In fact, severe plastic deformation (SPD) techniques are known to produce bulk metallic materials with fine-grained structure [2]. Among the various SPD techniques, equal channel angular pressing (ECAP) is able to result in grain sizes typically in the range of 400-800 nm[3-13]. In particular, ECAP is an especially attractive processing method because it allows large bulk samples to be produced, which are free from any residual porosity, and are subjected to small shape changes. During shearing deformation, the evolution and accumulation of misorientation across both low-angle boundaries (LABs) and high-angle boundaries (HABs) is closely related to the crystallographic accommodation of each crystallite with its neighbouring crystallites [10,12]. Thus, plastic deformation of metals occurs as a result of the formation, movement and storage of dislocations.

Several approaches to model the material yield stress, starting from the microstructure strengthening contributions, have been proposed [14-23]. Different authors have reported studies on the combined effect of ultrafine structure and deformation-induced segregation of solute elements at grain boundary. Moreover, in different published works [16-19,24-32] in addition to dislocation and particle strengthening, a contribution from solid solution (solute elements) was recognised and properly addressed.

In these and other studies,mostly on aluminum and in some cases, on titanium alloys [6,7,9,14,15,18-23,33-41], the combination of grain boundary and Orowan-type strengthening contributions were addressed. It was exhaustively documented that dislocation sliding is the major deformation mechanism that is ultimately responsible for the majority of the material yield stress.

The 2xxx series heat treatable aluminium alloys are widely used because of their high strength to weight ratios. The AA2219 alloy has a great potential for a wide range of applications owing to its high specific-strength, good fracture toughness and excellent stress-corrosion resistance [42-44]. The mechanical properties of this alloy are strongly influenced by the alloying elements (Fe,Mn,Ni, Cu, and Cr) since most of them take part to the formation of intermetallic compounds characterized by high thermal stability and hardness value. Iron is one of the main impurities in aluminium alloys and its solid solubility in Al is very low, resulting in the formation of intermetallic compounds, whose

Marcello Cabibbo
Dipartimento di Ingegneria Industriale e Scienze Matematiche (DIISM)
Università Politecnica delle Marche, Via Brecce Bianche, 60131-Ancona

nature strongly depends on other impurities or alloying elements. The presence of iron is quite harmful because of the tendency to form brittle AlFeSi needle-like precipitates or platelets [44]. To avoid, or at least control, the precipitation of iron containing intermetallic compounds during alloy solidification, manganese is usually added [45]. Moreover, manganese is able to modify the type and the morphology of intermetallic phases, from platelets to cubic or globules. These latter morphologies result to be very important as they can improve the tensile strength, the elongation and the ductility of the considered alloy [45]. The AA2xxx-series are characterized by the formation of $(Fe,Mn)Al_6$ and $(Fe,Mn)_3Si_2Al_{15}$ intermetallic phases. $(Fe,Mn)Al_6$ is the one likely to form in the Al-Fe-Mn-Si system over wide range of commercial alloys. On the other hand, in many alloys, $(Fe,Mn)Al_6$ reacts peritectically with the liquid to form $(Fe,Mn)_3Si_2Al_{15}$. However, in high-silicon alloys, as AA2219, $(Fe,Mn)_3Si_2Al_{15}$ is considered the primary intermetallic phase [42]. These intermetallic particles act as secondary phase reinforcements to the matrix [43] (for further insights, the reader is referred to the cited textbooks [42] and [43]).
The present work focused on the strengthening effect of uniaxial severe plastic deformation (through ECAP route A) on a AA2219.

EXPERIMENTAL DETAILS

The AA2219 was pressed in the as-extruded (AE) condition, i.e. hot extrusion to 800 K followed by room temperature cooling. The alloy is characterized by a diffuse presence of fine strengthening $\theta(Al_2Cu)$ secondary phaseparticles. Cylindrical billets had a diameter of 9.8 mm and length of 10 cm.Cylindrical bars were pressed in a ECAP die consisted of two symmetrical half blocks of SK3 toolsteel of nominal hardness 45 HRC [46-51]. Route A implies no billet rotation between passes into theECAP die channels. Pressing speed was ~ 5 mms^{-1}.
Light microscopy (LM) inspections were carried out on surfaces polished and electrolytically etched with a solution consisting of 5 ml HBF4 in 200 ml distilled water, at 18V, and immersion time of less than a minute. Three different billet planes were characterized: extruded (XY), transverse (XZ), and section (YZ).
Polished samples were characterized with a highresolution scanning electron microscope (FEG-SEM). To distinguish the intermetallics from thematrix, the backscattered electrons (BSE) images were collected. In order to optimize the backscattered electron signal, observations were performed using a high accelerating voltage (15 kV). Quantitative stereological image analysis was performed according to the ASTM E112. In order to evaluate the strengthening contribution yield by the intermetallic phase particles, quantitative stereology analyses were performed. All the micrographs were taken in the YZ deformed plane (section).
Microstructure inspections were performed by transmission electron microscopy (TEM) with subsequent quantitative image analysis. Thin foils were sliced parallel to the longitudinal section of
the ECAP billets and prepared by mechanical polishing to surface flatness and twinjet electro-polishing in a solution of 30 %perchloric acid in methanol. The TEM was operated at 200 kV and equipped with a double tilt specimen holder. To measure boundary misorientation angles, Kikuchi line analysis was carried out in the TEM [48-56]. Most of the low-angle dislocation boundaries showed Moiré fringes. In such cases, a direct and straightforward misorientation angle measurement method was applied [54,55]. Boundary spacing was calculated using the linear intercept method. The average boundary intercept distance was calculated from the average orthogonal boundary intercept spacing, *LX* and *LY*, where the suffix *X* and *Y* stands for the two mutually orthogonal directions, *X* being oriented to be parallel to the ECAP direction. Therefore, the average boundary spacing $LXY = 1/NLXY$, where $NLXY = (1/LX + 1/LY)/2$ is the number of boundary intercepts per unit of test line length along *X* and *Y*. Thus, the total boundary surface per unit volume, *SV*, is $SV = 2/LXY$. The terms low-angle boundary (LAB) and high-angle boundary (HAB) refer to the generation, induced by the ECAP shear deformation, of crystallites having the character of cell and grain, respectively. All the existing nanometric strengthening agglomerates and particles, i.e. the GP-I, GP-II (θ”), and the θ’phases formed during the short adiabatic heating promoted by the ECAP, and the equilibrium $\theta(Al_2Cu)$ phase formed during the hot extrusion prior ECAP, were characterized in terms of their mean size, volume fraction, and spacing. These were measured by standard stereological methods (see for instance [57,58]).
Microhardness measurements were performed using a load of 100 gf along the three different sample planes, i.e.: XY, XZ, and YZ. The first two planes were sectioned at approximately 0.3 mm from the cylindrical bar surfaces. Tensile tests were carried out on a standard load frame equipped with a sample extensometer.
The different microstructure strengthening contributions were identified and discussed. There are three factors that contribute to the overall microstructure strengthening for this alloy:
- an aluminum matrix term, $\sigma_{pure\ Al}$ = 10 MPa [52], which refers to un-textured, undeformed and very coarse grained pure aluminum.
- a dislocation term, coming from a linear combination of the high-angle boundaries (HABs, i.e. grains), the low-angle boundaries (LABs, i.e. cells), and the very-low-angle boundaries (those showing Moiré fringes on TEM) during ECAP.
- a strengthening term coming from the agglomerate and pre-precipitate particles generated by the ECAP-induced adiabatic heating, that is from the GP-I, GP-II (θ”), and the semi-coherent θ’ pre-precipitate. These are indeed induced to form by the combined effect of the adiabatic heating generated during the ECAP deformation and the newly introduced tangle dislocation within the deforming

grains and cells. The GP agglomerates and the semi-coherent θ' pre-precipitates are thus generated along the tangle dislocations.The contribution coming from the equilibrium θ = Al_2Cu secondary phase particles is modelled according to shearable (cut) and non-shearable (bypass) character, which is determined by their size.
- a further intermetallic strengthening contribution, which is determined by FEGSEM inspections out of unetched polished surfaces, and modelled according to the shear-lag model first proposed by Nardone and Prewo [59].
All the microstructure features that contribute to the alloy yield stress are reported in Fig. 1.

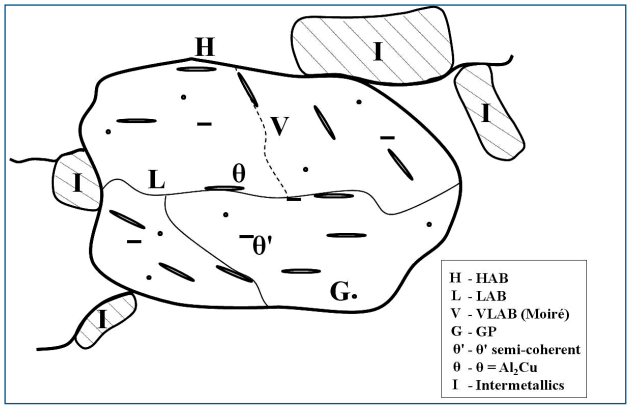

Fig. 1 - Scheme of the microstructure features that contribute to the alloy yield stress, after ECAP.

EXPERIMENTAL RESULTS

The light microscopy inspections on the As Extruded (AE) alloy, after ECAP/A-1 pass and after ECAP/A-2 passes showed a grain size reduction accounting for 15% in the XY (extruded) plane. In the same plane, further ECAP pass reduced the grain size by 10%, respect to the 1-ECAPgrain size. This small grain size reduction, from1 to 2 passes, was also observed in the XZ (transverse) and YZ (section) planes.
The microhardness profiles recorded along the three different sample planes (XY,XZ, YZ) showed a dramatic hardness increment at the first ECAP pass with respect tothe as-extruded condition, being the hardness rose by less than 20% with further accumulative strain (ε= 1.08 to 2.16). The hardness profiles along the sample plane sections XY and XZ did not show anysignificant difference.
All the existing equilibrium θ(Al_2Cu) particle formed, mostly along the grain boundaries and thecell boundaries, during hot extrusion (800 K) and subsequent room temperature cooling. DuringECAP, it is apparent that the microstructure grain and cell reduction with strain, is accompanied bya partial dissolution process of the equilibrium θ(Al_2Cu) particles[46,60].
Figure 2 documents the presence of GP-I, GP-II (θ"), and the semi-coherent θ' which were formedby the adiabatic heating generated during the passage of the billet through the L-shaped equalchannel of the die.
It is worth to note that the agglomerate and pre-precipitate formation is also strongly promoted by the tangle dislocation formed during ECAP, as shown by the larger presence after the second pass (Fig. 2(b)), compared to the microstructure after the first pass (Fig. 2(c)). The ECAP-induced adiabatic heating and tangle dislocations promote the generation of the GP-I, GP-II (θ"), and the semi-coherent θ' along the newly introduced dislocations.
Fig.3 shows representative FEGSEM micrographs of the intermetallic phases in the three examined conditions: AE (Fig.3(a)), at ECAP/A-1 (Fig.3(b)) and at ECAP-/A-2 (Fig.3(c)). All the micrographs reported in Figure 3 have been collected in backscattered electrons (BSE) mode at a voltage of 15 keV. In Figure 3, the darker portions are the aluminum matrix, while the brightest zones are the intermetallics. The area of every precipitate in the micrographs was measured by animage analysis software package and the data were analyzed using the area analysis (AA) stereology method of quantification [53], based on the Woodhead's coefficients [57] for the calculation of the particle sizedistribution.

DISCUSSION

Solid solution strengthening

The presence of solute atoms within the alloy matrix cause a drag effect against dislocation motion, thus contributing as a matrix strengthening. Several elements are potentially located in solid solution, these are:Cu, Fe, Si, Mn, and Cr. Anyhow, Fe, Cr, and the vast majority of the Mn and Si contribute to the formation of the $(Fe,Cr,Mn)_3Si_2Al_{15}$intermetallic phases. A small fraction of the Mn and Si atoms, together with the more abundant Cu, do contribute to the alloy strengthening by [34]. The solute element concentration of Si and Mn within the matrix remained essentially unchanged with the accumulative strain.For the Cu solid solution concentration and the related contribution to the alloy yield strength two concurrent microstructure phenomena induced by the severe plasticdeformation take place: (i) the changing strengthening contribution of the Al2Cu secondaryparticles, which are induced to be cut away by sliding dislocations as the deformation accumulates, and (ii) the generation of fine GP zones and semi-coherentθ' particles by the adiabatic heating generated during ECAP [56].

Dislocation boundary and secondary phase strengthening

The flow stress can be assumed to be expressed as the sum of boundary strengthening, according to the classical Hall-Petch relationship, and dislocation cell (either low-angle and very-low-angle boundary) strengthening [38,39,43,44,62,63,64].
Therefore the HAB contribution was calculated as Hall-Petch strengthening, while the LAB strength contribution was considered proportional to the square root of the density of dislocation stored in the boundaries

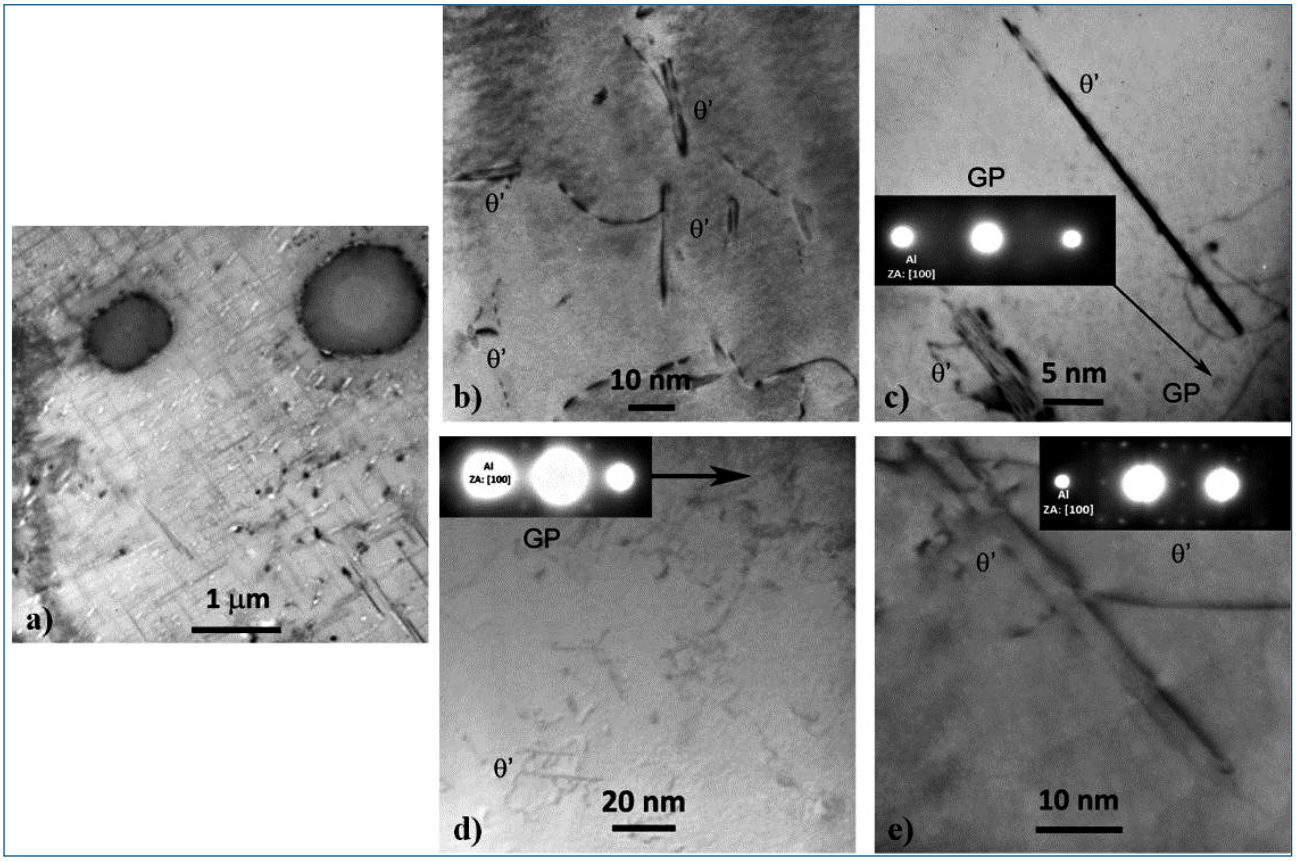

Fig. 2 - Typical microstructure of the as-extruded (AE) alloy condition in which a diffuse presence of plate-likeequilibrium θ (Al2Cu) secondary phase particles are documented along with two rounded(Fe,Mn,Cr)3Si2Al15 intermetallic particles, a). GP-I, GP-II (θ"), and semi-coherent θ' particles induced bythe adiabatic heating, in ECAP-1, b), c); and in ECAP-2, d),e). SAEDPs document the nature of GP-II (θ")agglomerates (in c) and d)), and the θ' pre-precipitate particles (in e)).

[38,43,44,63,64]. A further strengthening contribution, coming from the very-low-angle boundary cells (i.e. those showing Moiré fringes on the TEM) was also extracted from the rest of the low-angle boundary contribution.
Non-shearable (bypassed) particles contribute to the alloy strengthening through the Orowan strengthening mechanism[65].

Adiabatic heating induced GP-I, GP-II (θ"), and semi-coherent θ' strengthening

The reported low fraction of the GP zones and the even lower fraction of the semi-coherent θ' particles, with respect to the equilibrium θ phase, is chiefly due to the rather short time of thermal exposure of the billet in the adiabatic heating zone during ECAP. According to [67], the duration of the heating excursion from room temperature, on the passage of the billet through the shearing plane, is typically less than 8-10 s for ram speed of 18 mm×s^{-1}. Assuming that the heating duration decreases with the ram speed, it is thus possible to assume a time of adiabatic heating of some 8 s, at a ram speed of 5 mm×s^{-1}, as in the present case.
According to Kim [68], the temperature rise, ΔT, of the billet in the specific zone subjected to the shear deformation during ECAP, that is the billet volume at, and immediately behind and ahead, the L-shape channel of angle Φ and a die corner curvature Ψ, can be written as, Eq. (1):

$$\Delta T = \frac{0.9\sigma\varepsilon + 0.5m\left(\frac{\sigma}{\sqrt{3}}\right)u\frac{A}{V}\Delta t}{\rho C + \frac{A}{V}h\Delta t}$$

where σ is the saturation stress, $\varepsilon$is the strain developed during ECAP, m is the friction factor (which can be assumed equals to 0.2, for the Mo_2S lubricant used for the ECAP), u = 5 mm×s^{-1} is the ram speed, A is the surface area of the deformation zone ($A = \pi^2 d^2(\Phi/2\pi)$, where d = 9.8mm is the diameter of the cylindrical billet, and $\Phi = \pi/2$), V is the volume of the deformation zone ($V = (\pi^2/4) d^3(\Phi/2\pi)$), $\Delta t = (d/u)(\Psi/\sqrt{2}\pi)$, with $\Psi = \pi/4$, is the average dwell time of the adiabatic heating experienced by the deformation zone, ρ= 2.85 g×m^{-3} is the alloy density, C = 0.205 Cal×kg^{-1}×K^{-1}is the alloy heat capacity, and h = 2000 N×m^{-1}×s^{-1} is the heat transfer coefficient of aluminum. The adiabatic dwelling time, Δt, gives information on the exposition duration to the adiabatic heating, by the deforming alloy, during ECAP. The peak temperatures are lower than T= 400 K, in both ECAP-1 and ECAP-2 and in good agreement to those reported in [66,68] for other aluminum al-

loys. The GP formation temperature is in the range of 330-360 K for the AA2219., while the formation temperature of the semi-coherent θ' is much higher, being of some 700 K [68] (and references therein). Thus, the low concentration of GP zones detected within the matrix and along the tangle dislocations is likely due to the fact that the adiabatic heating experienced by the alloy during ECAP was below the GP formation temperature range. The presence of few θ' is believed to be justified by the combined effect of the severe plastic deformation (partial and complete secondary phase fragmentation, and promotion of fast formation of precipitation sequence induced by the large dislocation density introduced), by the adiabatic heating (local heating), and by local high solute concentration within the aluminum matrix [60]. Lochte *et al.* reported [69] that the formation of a certain amount of GP zones, in Al-Cu alloys, at temperatures as low as 420 K, requires dwelling times of about 60 s. These temperatures and dwelling time generate very small GP zones of some 2-3 nm-long.
The strengthening contribution of both the GP zones and the semi-coherent θ' particles are determined according to the anti-phase boundary strengthening mechanism. The rather small size of GP zones, with a mean equivalent diameter of less than 4 nm, and of the θ' particles, for which the mean equivalent diameter is within the 22 nm, make this assumption suitable. The very low fraction and rather limited size of both GP zones and, to a much extent, of the θ' particles, account for the rather low strengthening contribution.

Intermetallic strengthening contribution

Fig.3 shows representative FEG-SEM micrographs of the intermetallic phases in the AE (Fig. 3(a)), ECAP/A-1 (Fig. 3(b)), and ECAP/A-2 (Fig. 3(c)) conditions. The FEG-SEM observations revealed large intermetallics in the alloy structure. The results obtained by using thearea analysis (AA) stereology methodof quantification [57,61] suggest that the shearing deformation did not introduce a significant shear of the intermetallic particles and it did not alter their aspect ratio, .It can be pointed out that there is a rearrangement of the intermetallic phases that follows the rearrangement of grains and subgrains.
As reported in literature, the presence of intermetallic compounds contribute to the alloy reinforcement [56]. In order to evaluate the effect of these compounds on the behaviour of the AA2219 alloy, a characteristic strengthening term was calculated. This one was the IPA parameter, which is literally the parameter of intermetallics appearance index, introduced by Shabestari *et al.* [70] and taking into account the geometric features and the volume spacing of the particles. The IPA parameter can be calculated as follows, Eq.(2):

$$IPA = \frac{\alpha d}{\lambda} \quad (2)$$

The definition of this term is linked to the probability of brittle fracture in a reinforced soft matrix, which depends only on the equivalent diameter of particles, *d*, on the aspect ratio, α, and on the intermetallic particles average

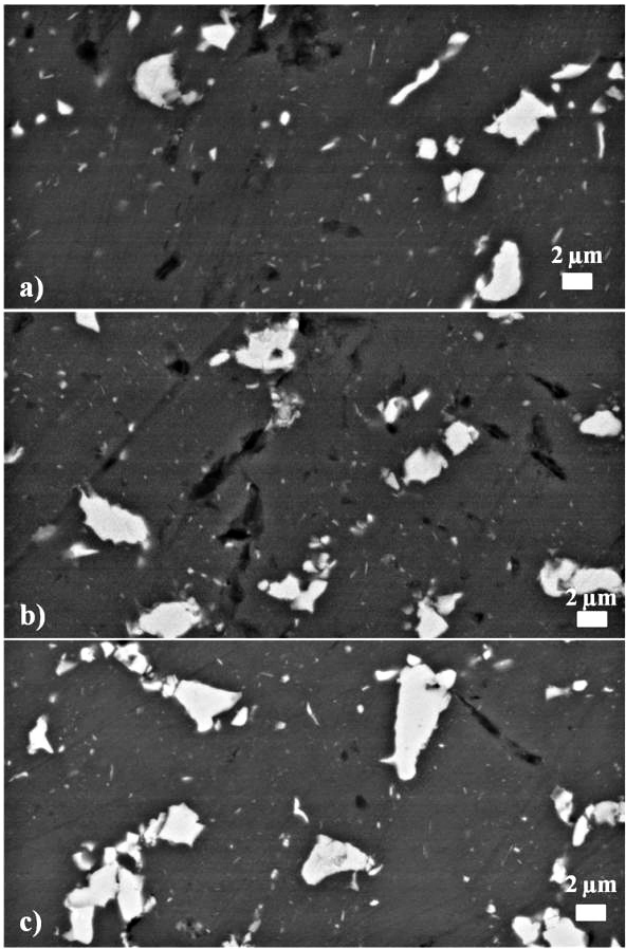

Fig. 3 - FEGSEM micrographs of the a) as-extruded condition, b) after ECAP/A-1 pass and c) after ECAP/A-2 passes, documenting the size and shape of the $(Fe,Mn,Cr)_3Si_2Al_{15}$ intermetallic.

distance, λ. The values of the intermetallics appearance index (IPA) raise at one ECAP pass with respect to the as-extruded condition, while being slightly different after ECAP/A-2, showing that the decrease in the IPA parameter is not strongly dependent on the rate of the imposed deformation.
According to the composite metal approach [71,72], a load transfer strengthening term, from the aluminum matrix to the iron-based intermetallic particles, could be linearly summed to the other microstructure strengthening contribution. Thus, the composite particles do contribute to alloy reinforcement carrying a fraction of the load from the matrix, $\Delta\sigma_{LT}$. This strengthening strongly depends on particle shape, morphology, and volume fraction; it specifically depends on the particle aspect ratio, as follows, Eq. (3), [73]:

$$\Delta\sigma_{LT} = \sigma_0 \left[1 + \left(\frac{(L+t)\alpha}{4L} \right) N_V \right] \quad (3)$$

where σ_0 is the un-reinforced matrix stress (flow stress), N_V is the intermetallic particle volume fraction, *L* is the long broader surface edge (the particle size facing the load

direction), *t* is the mean particle thickness and α is the particle aspect ratio. The intermetallic volume fraction, N_V, was determined using the already cited area analysis (AA) stereology method [61].
A further strengthening effect, can be calculated as proposed by Hazzledine *et al.* [73] by applying the following expression, Eq. (4):

$$\Delta\sigma_{\text{Intermet}} = \frac{MGb}{d}\left(\frac{6N_V}{\pi}\right) \quad (4)$$

where *d* is the intermetallic particle size (i.e., the diameter). This term is the specific contribution to the strengthening due to the presence of the intermetallic precipitates. The fraction, N_V, of intermetallic compounds present in the matrix is increased at ECAP/A-1 pass with respect to the AE results, while remaining substantially unchanged at ECAP/A-2. Similarly, the values of the strengthening terms $\Delta\sigma_{LT}$ and $\Delta\sigma_{Intermet}$ are increased at ECAP/A-1 pass but then remain substantially unchanged at ECAP/A-2 passes. This result fully agrees with literature [56]. This effect can be explained with the morphological modifications (the values of *L* and *t*) to which the intermetallic particles are subjected by the SPD.

Microstructure strengthening combination

According to several authors [17,19,25,27,29,34,56,74-76], the total strengthening microstructure contribution, coming from the different microstructure terms (solid solution, *ss* subscript, dislocation boundaries, *dislocation* subscript, and secondary phase, *secondary-phase* subscript), $\Delta\sigma_{ss+dislocation+secondary\text{-}phase}$, can be combined linearly: $\Delta\sigma_{ss+dislocation+secondary\text{-}phase} = \sigma_0 + \Delta\sigma_{ss} + \Delta\sigma_{SPD} + \Delta\sigma_{adiabatic\text{-}heating} + \Delta\sigma_{\theta=Al2Cu}$, where σ_0 is the un-texture aluminum matrix contribution, $\Delta\sigma_{ss}$ is the solid solution contribution, $\Delta\sigma_{SPD} = \Delta\sigma_{very\text{-}low\text{-}angle\ boundaries}$*(Moiré)* $+ \Delta\sigma_{LAB\text{-}Moiré} + \Delta\sigma_{HAB}$is the boundary strengthening induced by ECAP (very-low-, i.e. Moiré, low-, and high-angle boundary), $\Delta\sigma_{adiabatic\text{-}heating}$ is the contribution generated by the GP zones and θ' particles induced to precipitate by the adiabatic heating, $\Delta\sigma_{\theta=Al2Cu}$ is the$\theta=Al_2Cu$ particle strengthening.
The intermetallic particle contribution is a coarser feature, which is equally distributed throughout the entire alloy microstructure. Thus, the sub-micrometric and dislocation strengthening terms were combined quadratically to the coarser micrometric intermetallic particle contribution, according to Eq. (5):

$$((\Delta\sigma_{disl+spp})^2 + (\Delta\sigma_{LT} + \Delta\sigma_{intermet})^2)^{1/2} \quad (5)$$

In both the ECAP experimental conditions, excellent agreement between the calculated yield stress and the experimental stress obtained either through microhardness measurementsand by the measured stress, was obtained.

CONCLUSIONS

In the present work the microstructure intermetallics strengthening in a AA2219 aluminium alloy subjected to ECAP was studied. The material was investigated in the as-extruded condition, after one ECAP pass and after two ECAP passes using route A. Light microscopy investigations, microhardness measurements, transmission electron microscopy observations and scanning electron microscopy observations were carried out. Finally a quantitative stereology analysis was performed on the SEM micrographs.

- TEM inspections showed a dramatic grain size reduction at the first ECAP pass, accounting for one order of magnitude, followed by a much lower size reduction at the second pass.
- The adiabatic heating induced the formation of GP-I, GP-II (θ''), and eventual few semi-coherent θ' pre-precipitates.
- The precipitation of GP and θ' was promoted to occur along the newly introduced tangle dislocation during ECAP.
- A detailed microstructure strengthening model able to meet, almost perfectly, the measured alloy yield stress determined experimentally and through microhardness measurements, was here developed.

CONCLUSIONI

Il presente lavoro è dedicato ad uno studio microstrutturale di una lega AA2219 sottoposta ad ECAP. La lega è stata studiata nella sua condizione come-estruso, dopo 1 e 2 passate ECAP, mediante la modalità A. Sono state utilizzate tecniche di indagine microstrutturale quali microscopia ottica, FEGSEM, e TEM. Quantificazioni stereologiche hanno consentito di ottenere i seguenti risultati:

- Notevole riduzione delle dimensioni medie dei grani cristallini già dopo la prima passata ECAP (riduzione di un ordine di grandezza) e conseguente più modesto tasso di riduzione alla seconda passata.
- Il calore adiabatico sviluppato durante il processo ECAP ha indotto la formazione di fasi intermedie quali: GP-I, GP-II (θ''), e, seppur modesta, una frazione di particelle semi-coerenti θ.
- La precipitazione delle fasi GP e θ' è stata promossa dalla presenza diffusa di dislocazioni libere generate dalla deformazione plastica di taglio durante il passaggio nello stampo ECAP.
- È stato proposto ed applicato un modello di combinazione di tutti i contributi microstrutturali al rafforzamento della lega, in grado di descrivere con ottima approssimazione la resistenza a snervamento della lega dopo 1 e 2 passate ECAP mediante la modalità A.

RIFERIMENTI BIBLIOGRAFICI

[1] N. HANSEN, X. HUANG, D.A. HUGHES, Mater. Sci. Eng. A317 (2001) 3.
[2] R.Z. VALIEV, T.G. LANGDON, Prog. Mater. Sci. 51 (2006) 881.

[3] P. LUO, D.T. McDONALD, W. XU,S. PALANISAMY, M.S. DARGUSCH, K. XIA, Scripta Mater. 66 (2012) 785.
[4] X. SAUVAGE, G. WILDE, S.V. DIVINSKI, Z. HORITA, R.Z. VALIEV, Mater. Sci. Eng. A540 (2012) 1.
[5] W. YUAN, S.K. PANIGRANHI, J.-Q. SU, R.S. MISHRA, Scripta Mater. 65 (2011) 994.
[6] S. DADBAKHSH, A.K. TAHERI, C.W. SMITH, Mater. Sci. Eng. A527 (2010) 4758.
[7] A. SHAN, I.G. MOON, J.W. PARK, J. Mater. Proc. Techn. 122 (2002) 255.
[8] C. XU, M. FURUKAWA, Z. HORITA, T.G. LANGDON, Mater. Sci. Eng. A398 (2005) 66.
[9] E.A. EL-DANAF, Mater. Design 32 (2011) 3838.
[10] P.N. BERBON, T.G. LANGDON, TMS (The Minerals, Metals & Materials Society), Warrendale, PA (2000) 381.
[11] Y. IWAHASHI, J. WANG, Z. HORITA, M. NEMOTO, T.G. LANGDON, Scripta Mater. 35 (1996) 143.
[12] D.A. HUGHES, Mater. Sci. Eng. A319-321 (2001) 46.
[13] A. GHOLINIA, P.B. PRANGNELL, M.V. MARKUSHEV, Acta Mater. 48 (2000) 1115.
[14] R. DOBSZ, M. LEWANDOWSKA, K.J. KURZYDLOWSKI, Comp. Mater. Sci. 53 (2012) 286.
[15] R. DOBSZ, M. LEWANDOWSKA, K.J. KURZYDLOWSKI, Scripta Mater. 67 (2012) 408.
[16] A.S. TAHA, F.H. HAMMAD, Phys. Stat. Sol. (a) 119 (1990) 455.
[17] T. SHANMUGASUNDARAM, M. HEILMAIER,B.S. MURTY,V.S. SARMA, Mater. Sci. Eng. A527 (2010) 7821.
[18] E.I. HUSKINS, B. CAO, K.T. RAMESH, Mater. Sci. Eng. A527 (2010) 1292.
[19] M. DIXIT, R.S. MISHRA, K.K. SANKARAN, Mater. Sci. Eng. A478 (2008) 163.
[20] Y. ITO, Z. HORITA, Mater. Sci. Eng. A503 (2009) 32.
[21] D. ORLOV, Y. BEYGELZIMER, S. SYNKOV, V. VARYUKHIN, N. TSUJI, Z. HORITA, Mater. Sci. Eng. A519 (2009) 105.
[22] K.J. KURZYDLOWSKI, J.J BUCKI, Acta Metall. Mater. 42 (1993) 3141.
[23] R.Z. Valiev, E.A. ENIKEEV, M.Y. MURASHKIN,V.U. KARZYKHANOV, X. SAUVAGE, Scripta Mater. 63 (2010) 949.
[24] S. ZHANG, W. HU, R. BERGHAMMER,G. GOTTSTEIN, Acta Mater. 58 (2010) 6695.
[25] F. TANG, D.S. GIANOLA, M.P. MOODY, K.J. HEMKER, J.M. CAIRNEY, Acta Mater. 60 (2012) 1038.
[26] O.R. MYHR, Ø. GRONG, S.J. ANERSEN, Acta Mater. 49 (2001) 65.
[27] M.J. STARINK, P. WANG, I. SINCLAIR,P.J. GREGSON, Acta Mater. 47 (1999) 3855.
[28] C. SCHLESIER, E. NEMBACH, Acta Metall. Mater. 43 (1995) 3983.
[29] H.R. SHERCLIF, M.F. Ashby, Acta Metall. Mater. 38 (1990) 1789.
[30] A.J. ARDELL, Met. Trans. 16A (1985) 2131.
[31] P. GOMIERO, Y. BRECHET, F. LOUCHET, A. TOURABI, B. WACK, Acta Metall. Mater. 40(1992) 857.
[32] K.L. KeENDIG, D.B. MIRACLE, Acta Mater. 50 (2002) 4165.
[33] K. OKAZAKI, H. CONRAD, Acta Metall. 21(1973) 1117.
[34] N. KAMIKAWA, X. HUANG, N. TSUJI, N. HANSEN, Acta Mater. 57(2009) 4198.
[35] Q. LIU, X. HUANG, D.J. LLOYD,N. HANSEN, Acta Mater. 50(2002) 3789.
[36] R. UEJI, X. HUANG, N. HANSEN, N. Tsuji, Y. MINAMOTO, Mater. Sci. Forum 426-432 (2003) 405.
[37] J.R. BOWEN, P.B. PRANGNELL, D. JUUL JENSEN, N. HANSEN, Mater. Sci. Eng. A387-389 (2004) 235.
[38] N. HANSEN, X. HUANG, R. UEJI,N. TSUJI, Mater. Sci. Eng. A387-389 (2004) 191.
[39] N. HANSEN, Scripta Mater. 51(2004) 801.
[40] N. HANSEN, Mater. Sci. Eng. A409(2005) 39.
[41] H.S. KIM, Y. ESTRIN, Mater. Sci. Eng. A410-411 (2005) 285.
[42] L.F. MONDOLFO, Manganese in Aluminum Alloys. The Manganese Center, Paris, (1978).
[43] J.E. HATCH, Aluminum properties and physical metallurgy. American society for metals, Metals Park, Ohio, (1984).
[44] G. ALBERTINI, G. BRUNO, B.D. DUNN, F. FIORI,W. REIMERS, J.S. WRIGHT, Mater. Sci. Eng. A224 (1997) 157.
[45] S.G. SHABESTARI, Mater. Sci. Eng. A383 (2004) 289.
[46] M. CABIBBO, E. EVANGELISTA, M. VEDANI, Metall. Mater. Trans. A36 (2005) 1353.
[47] M. VEDANI, P. BASSANI, M. CABIBBO,V. LATINI,E. EVANGELISTA, Metall. Sci. Techn. 21 (2003) 3.
[48] M. CABIBBO, Mater. Charact. 61 (2010) 613.
[49] V.M. SEGAL, Mater. Sci. Eng. A197 (1995) 157.
[50] M. FURUKAWA,Y. IWAHASHI,Z. HORITA, M. NEMOTO,T.G. LANGDON, Mater. Sci. Eng. A257 (1998) 328.
[51] V.M. SEGAL, Mater. Sci. Eng. A338 (2002) 331.
[52] Q. LIU, J. App. Cryst. 27(1994) 755.
[53] Q. LIU, Ultramicroscopy 60(1995) 81.
[54] D.B. WILLIAMS, C.B. CARTER, Transmission Electron Microscopy. Vol. II - Diffraction. Plenum Press, New York, 1996.
[55] M. CABIBBO, W. BLUM,E. EVANGELISTA,M.E.KASSNER, M.A. MEYERS, Metall.Mater. Trans. 39A(2008) 181.
[56] M. CABIBBO, Mater. Sci. Eng. A560 (2013) 413.
[57] D.A. HUGHES, N. HANSEN, Acta Mater. 48(2000) 2985.
[58] R.L. HIGGINSON, C.M. SELLARS, Worked examples in quantitative metallography. Maney Publishing, London, (2003).
[59] V.C. NARDONE, K.M. PREWO, Scripta Metall. 20(1986) 43.
[60] M. CABIBBO, Mater. Charact. 68 (2012) 7.
[61] K.J. KURZYDLOWSKI, B. RALPH, The quantitative description of the microstructure of materials. CRC series in Materials Science and Technology, Uxbridge, UK, (1995).
[62] J.R. BOWEN, P.B. PRANGNELL,D. JUUL JENSEN, N.HANSEN, Mater. Sci. Eng. A387-389(2004) 235.
[63] J.H. DRIVER, D. JUUL JENSNEN,N. HANSEN, Acta Metall. Mater. 42(1994) 3105.
[64] N. HANSEN,X. HUANG, Acta Mater. 46(1998) 1827.
[65] J.W. MARTIN, Micromechanisms in Particle-Hardening Alloys. Cambridge Solid State Science Series, Cambridge (1980).
[66] D. YAMAGUCHI, Z. HORITA,M. NEMOTO,T.G. LANGDON, Scripta Mater. 41 (1999) 791.
[67] H.S. KIM, Mater. Trans. 42 (2001) 536.
[68] S.D. DUMOLT, D.E. LAUGHLIN, J.C. WILLIAMS, First Intl. Aluminum Welding Conference: Welding research Council. (1982) 115.
[69] L. LOCHTE, A. GITT,G. GOTTSTEIN, I. HURTADO, Acta Mater. 40 (2000) 2969.
[70] S.G. SHABESTARI, M. GHANBARI, J. Alloys Compd. 508 (2010) 315.
[71] N. LIHOLT, Risø Nat. Lab., Roskilde, Denmark, (1983) 381.
[71] T. CLYNE,P.J. WHITHERS,An Introduction to Metal Matrix Composites.CambridgeSolidState Science Series, Cambridge (1993).
[73] P.M. HAZZLEDINE, Scripta Metall. Mater. 26 (1992) 57.
[74] U.F. KOCKS, A.S. ARGON, M.F. ASHBY, Thermodynamics and Kinetics of Slip. Prog. Mater. Sci. 19, Pergamon Press, Oxford (1975).
[75] H. ADACHI, K. OSAMURA, S. OCHIAI, J. KUSUI, K. YOKOE, Scripta Mater. 44 (2001)1489.
[76] M. CAI, D.P. FIELD,G.W. LORIMER, Mater. Sci. Eng. A373(2004) 65.